Bulletin of the Seismological Society of America, Vol. 94, No. 6B, pp. S360–S369, December 2004

Triggered Deformation and Seismic Activity under Mammoth Mountain in Long Valley Caldera by the 3 November 2002 M_w 7.9 Denali Fault Earthquake

by M. J. S. Johnston, S. G. Prejean, and D. P. Hill

Abstract The 3 November 2002 M_w 7.9 Denali fault earthquake triggered deformational offsets and microseismicity under Mammoth Mountain (MM) on the rim of Long Valley caldera, California, some 3460 km from the earthquake. Such strain offsets and microseismicity were not recorded at other borehole strain sites along the San Andreas fault system in California. The Long Valley offsets were recorded on borehole strainmeters at three sites around the western part of the caldera that includes Mammoth Mountain—a young volcano on the southwestern rim of the caldera. The largest recorded strain offsets were -0.1 microstrain at PO on the west side of MM, 0.05 microstrain at MX to the southeast of MM, and -0.025 microstrain at BS to the northeast of MM with negative strain extensional. High sample rate strain data show initial triggering of the offsets began at 22:30 UTC during the arrival of the first Rayleigh waves from the Alaskan earthquake with peak-to-peak dynamic strain amplitudes of about 2 microstrain corresponding to a stress amplitude of about 0.06 MPa. The strain offsets grew to their final values in the next 10 min. The associated triggered seismicity occurred beneath the south flank of MM and also began at 22:30 UTC and died away over the next 15 min. This relatively weak seismicity burst included some 60 small events with magnitude all less than $M = 1$. While poorly constrained, these strain observations are consistent with triggered slip and intrusive opening on a north-striking normal fault centered at a depth of 8 km with a moment of 10^{16} N m, or the equivalent of a M 4.3 earthquake. The cumulative seismic moment for the associated seismicity burst was more than three orders of magnitude smaller. These observations and this model resemble those for the triggered deformation and slip that occurred beneath the north side of MM following the 16 October 1999 M 7.1 Hector Mine, California, earthquake. However, in this case, we see little post-event slip decay reflected in the strain data after the Rayleigh-wave arrivals from the Denali fault earthquake and onset of triggered seismicity did not lag the triggered deformation by 20 min. These observations are also distinctly different from the more widespread and energetic seismicity and deformation triggered by the 1992 M 7.3 Landers earthquake in the Long Valley caldera. Thus, each of the three instances of remotely triggered unrest in Long Valley caldera recorded to date differ. In each case, however, the deformation moment inferred from the strain meter data was more than an order of magnitude larger than the cumulative moment for the associated triggered seismicity.

Introduction

The Denali fault earthquake (Fig. 1) occurred at 22:12 UTC on 3 November 2002 on the Denali and Totschunda faults in central Alaska. It was a complex event that began on the Susitna Glacier Fault, ruptured eastward on the Denali fault, then southeast on the Totschunda Fault in a right-lateral sense. The total fault length was about 290 km of the Denali/Totschunda Fault and about 40 km of the Susitna Glacier Fault with a maximum surface rupture of 8.8 m (Eberhart-Phillips *et al.*, 2003; Haeussler, 2003). This event triggered earthquakes throughout the western United States and Canada primarily in regions of volcanic and geothermal activity (Gomberg *et al.*, 2001; Moran *et al.*, 2003; Husker

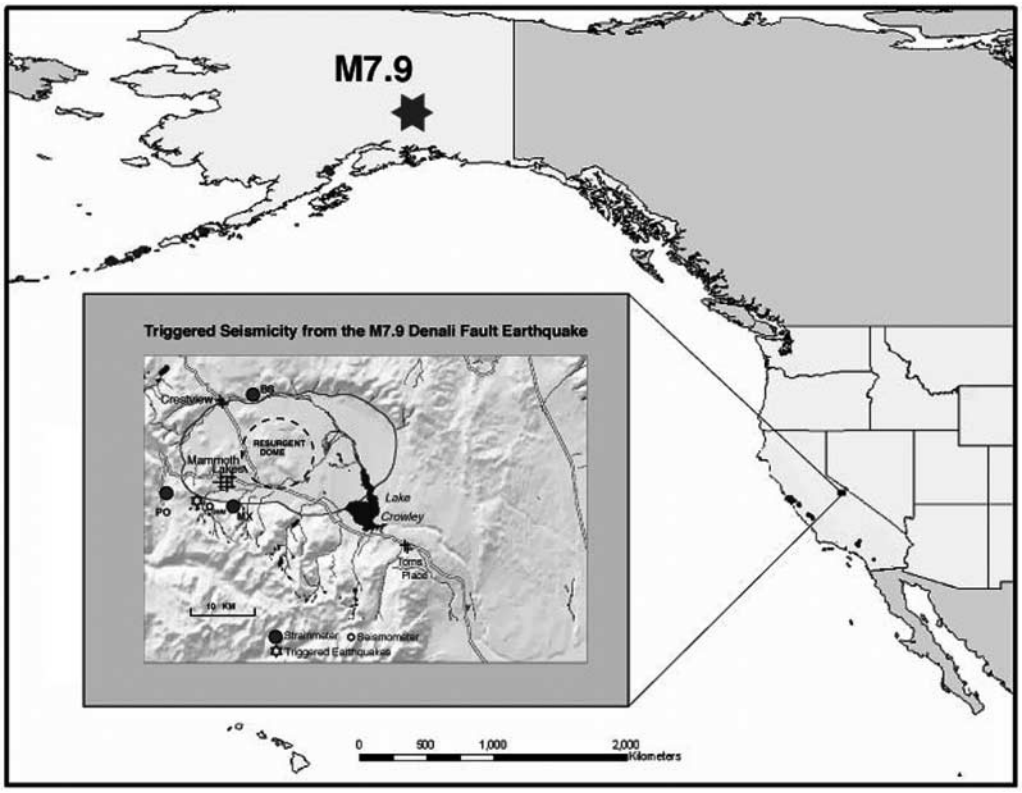

Figure 1. Location of the 3 November 2002, Denali fault earthquake (M_w 7.9) in relation to Long Valley caldera. The epicenter of the earthquake is shown as a star and the locations of borehole strainmeter sites (circles) along the San Andreas fault. Inset shows borehole dilatometer strain sites (circles) in Long Valley that recorded coseismic strain offsets at 22:30 during the arrival of Love and Rayleigh waves from 3 November 2002 Denali fault earthquake (M_w 7.9). The location of triggered seismicity in Long Valley is shown by a small star and the nearby broadband seismometer OMM by a small circle.

and Brodsky, 2004; Pankow *et al.*, 2004; Prejean *et al.*, 2004). One of these regions was Mammoth Mountain (MM) on the rim of Long Valley caldera, an active caldera in eastern California on the west side of the Sierra Nevada. In contrast to the 1992 Landers earthquake, which triggered large deformational moment release (Linde *et al.*, 1994; Johnston *et al.*, 1995) and extensive swarm activity in Long Valley caldera (Hill *et al.*, 1993; Anderson *et al.*, 1994) and elsewhere (Hill *et al.*, 1993; Gomberg *et al.*, 2001), this event produced a much smaller local strain transient and minimal triggered seismicity located under the south flank of MM. The Denali fault earthquake triggered response in Long Valley has both similarities and differences to that produced by the 16 October 1999, *M* 7.1 Hector Mine earthquake. For the Hector Mine earthquake, triggered deformation occurred under the north flank of MM during the largest surface wave arrivals with triggered seismicity following 20 minutes later (Johnston *et al.*, 2000). For Denali, triggered deformation occurred simultaneously with seismicity under the south flank of MM during the largest surface wave arrivals.

The importance of the Long Valley triggered deformation and seismicity records lies in the fact that this is the only site of remotely triggered activity where high resolution strain data is collected simultaneously with seismic data. This allows a more complete investigation of the physical mechanism(s) associated with the triggering process. In the case of the Landers triggering, the possible triggering mechanisms in volcanic regions include bubble mobilization in magma by large-amplitude surface-wave stresses (Linde *et al.*, 1994, Brodsky *et al.*, 1998), triggered fluid flow and diffusion of hydrothermal fluids by large-amplitude surface-wave stresses (Johnston *et al.*, 1995), and triggered slip on a deep fault beneath the region (Hill *et al.*, 1995). We note that of all locations (20) in California where simultaneous strain and seismic data are collected, records of triggered seismicity and deformation have been obtained only within the Long Valley caldera magmatic system. Other continuous strain sites are distributed along the San Andreas fault system (see Fig. 1).

This article describes triggered deformation and seismicity beneath MM from the 3 November 2002 M_w 7.9 Denali fault earthquake. We investigate the onset of triggering within the teleseismic wave arrivals, the likely source size and location of the triggered deformational event and related

seismicity and discuss the most likely physical mechanisms that may contribute to triggering. In this particular case, it appears that some combination of amplitude and frequency content of teleseismic waves is the driving mechanism. We show that triggered deformation (slow or silent earthquake) and seismicity follow the large amplitude Rayleigh-wave arrivals that have peak dynamic stresses of about 0.06 MPa. The silent earthquake and triggered seismicity are essentially over within 15 min of the Rayleigh-wave onset. The moment of the triggered deformation is three orders of magnitude greater than that released seismically. The silent earthquake may result from slip on a small normal fault with an equivalent magnitude of 4.3 at a depth of about 8 km under the south side of MM.

Instrumentation

We use seismic data from the broadband seismic station OMM installed in the Old Mammoth Mine and three Sacks-Evertson dilational strainmeters (Sacks *et al.*, 1971) installed at depths of about 200 m below the surface in bedrock at three sites BS, MX, and PO on the north, south, and west sides of Long Valley caldera, respectively (Fig. 1). Each borehole contains a strainmeter, a three-component accelerometer, and a three-component geophone. Furthermore, BS and MX each have a biaxial tiltmeter and pore-pressure monitors. The tilt data are not used here because of uncertainties in response. The strainmeters, installed as part of a cooperative program between the U.S. Geological Survey and the Carnegie Institution of Washington, are cemented in the borehole with expansive grout having physical characteristics approximating those of granite or sandstone host material. The remaining instruments are then installed above the strainmeters as the boreholes are filled to the surface with cement to minimize long-term strain changes due to hole relaxation, reequilibration of the aquifer system, and cable noise.

The data from the seismometers and dilatometers are sampled at 200 samples/sec and transmitted through a 24-bit Nanometrics satellite data collection system. The strain data are also transmitted with a 16-bit digital telemetry system through the Geostationary Operational Environmental Satellite (GOES) to Menlo Park, California, at 1 sample every 10 min (Silverman *et al.*, 1989). The sensors, the installation, and the telemetry system are calibrated together against the theoretical ocean-load corrected solid earth tides. This method of calibration is repeatable to better than 5%.

Remotely Triggered Deformation and Seismicity in Long Valley Caldera

Triggered seismicity beneath MM during the Denali fault earthquake wave train occurred in a tightly clustered burst of about 60 earthquakes beneath Horseshoe Lake on the south side of MM (shown as a small star in Fig. 1). The earthquakes all had magnitudes less than 1.0. These events were best recorded on the nearby broadband seismometer station OMM. Although only one earthquake was large enough to be located, similar waveforms indicate a similar location and depths (<4 km) of all these events (Prejean *et al.*, 2004).

Clear changes in strain were recorded on all three borehole dilatometers during the passage of the teleseismic surface waves through the region. The strain steps are shown in the five-day strain time history in Figure 2. For each instrument the raw data showing the solid earth tides (distinguished by their sinusoidal-like character) are plotted together with corrected data from which the predicted earth tides are removed (Tamura *et al.*, 1991). The data show clear steps with perhaps some hint of continued strain in the few hours following the event. The observed offsets for the three sites are −0.1 microstrain, 0.05 microstrain, and −0.025 microstrain at PO, MX, and BS, respectively. Compression is positive. The spikes on the strainmeter records result from aliased sampling of the straingram during the surface wave

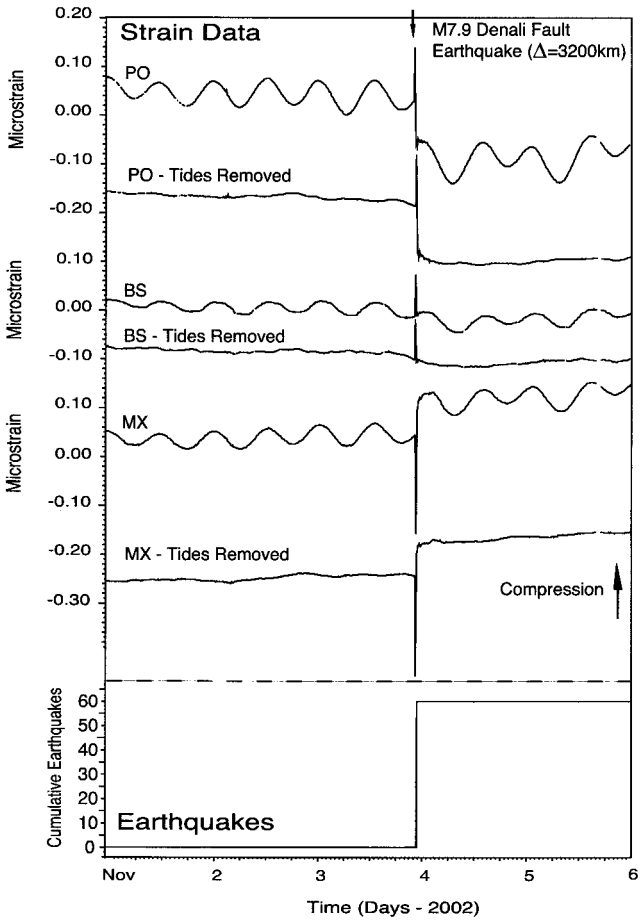

Figure 2. Raw (upper) and earth tide and atmospheric pressure corrected (lower) dilational strain data from each of the dilatometers PO, BS, and MX for a five-day period covering the 3 November 2002 M_w 7.9 Denali fault earthquake. Compression is positive. The lower plot shows the cumulative number of triggered earthquakes during this same time period.

train. Also shown in Figure 2 (bottom) is a plot of cumulative triggered seismicity.

Strain changes from teleseismic earthquakes are quite unusual. They have not been recorded by borehole strainmeters in tectonic regimes other than in the Long Valley caldera region, California, during the 22 years that this network has been operational. Furthermore, just three examples have been observed in Long Valley since 1984. The latest triggered strain steps in Long Valley clearly cannot be explained as source effects of the Denali fault earthquake because the expected static strains at this distance (3460 km) are less than 0.06 nanostrain (Okada, 1985, 1992). Furthermore, static strains from the Denali fault earthquake would be expected to have the same sign (extension) across the region rather than different signs, as observed. Thus, local triggered deformational appears to be the most likely explanation for these strain changes.

To better understand the triggered response and what might have initiated it, we investigate the details of the strain seismograms and triggered seismicity. Figure 3a shows an expanded version of the strain data for the 30 min before and 90 min after the arrival of the Denali fault teleseismic waves. The offsets evident in Figure 2 are still clear but are dominated by the surface wave train. It is evident even in these data that the offsets are not initiated by the *P*- and *S*-wave arrivals but later in the wave train, possibly by Love waves but most likely with the first Rayleigh-wave arrivals. The offsets are largely complete within the next 10 min as the Rayleigh wave train dies out. This is much clearer if these raw data are high-pass filtered (30-sec corner frequency) and the result subtracted from the original, as shown in Figure 3b. We use this procedure rather than a zero-phase low-pass filter to avoid the possibility of the filter modifying the long-period record. The onset appears to coincide with the first Rayleigh-wave arrival at 22:30 and grows relatively slowly during the next 7–10 min.

The onset of triggered earthquakes in relation to this slow deformation event can be seen in more detail by expanding the timescale to cover just the 22 min after the first *P*-wave arrival and comparing this with the onset of triggered seismicity evident in the east–west component of the high-frequency seismic wave train at OMM, the closest broadband seismometer, as shown in Figure 4. We choose this component since it best shows the onset and relative amplitude of the Love and Rayleigh waves. The triggered events clearly start near the beginning of the first large Rayleigh-wave arrival and the onset of the deformational event. They begin again with the next large arrival at 22:33 then continue in decreasing numbers until 22:40 UTC when the deformational event is largely complete.

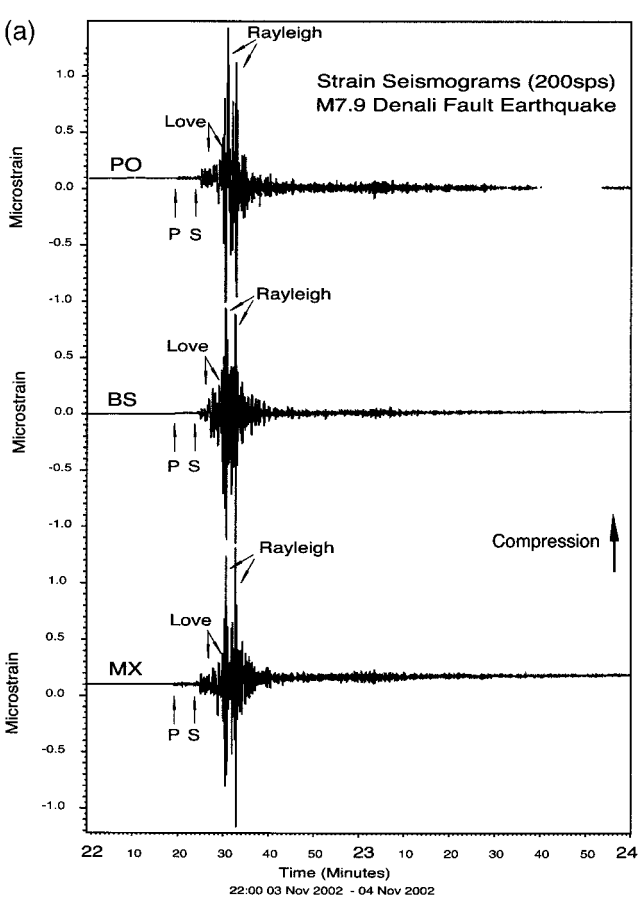

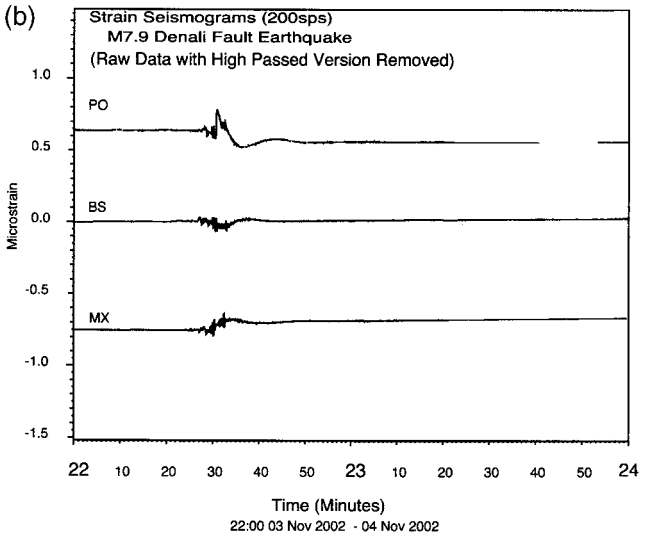

Figure 3. (a) Straingrams for a 2-hr period starting 20 min before the first *P*-wave arrival in Long Valley caldera from the 3 November 2002 M_w 7.9 Denali fault earthquake from each of the borehole strainmeters showing the various phases of the arriving teleseismic waves. (b) As for (a) except that the straingrams have all periods shorter than 30 sec (i.e., the normal seismogram) removed as a result of subtracting a high-pass-filtered version of the raw data. We use this procedure rather than a zero-phase low-pass filter to avoid the possibility of the filter modifying the long-period record. Data gaps in the PO record indicate missing data. Gaps were interpolated before filtering and interpolated sections removed after filtering.

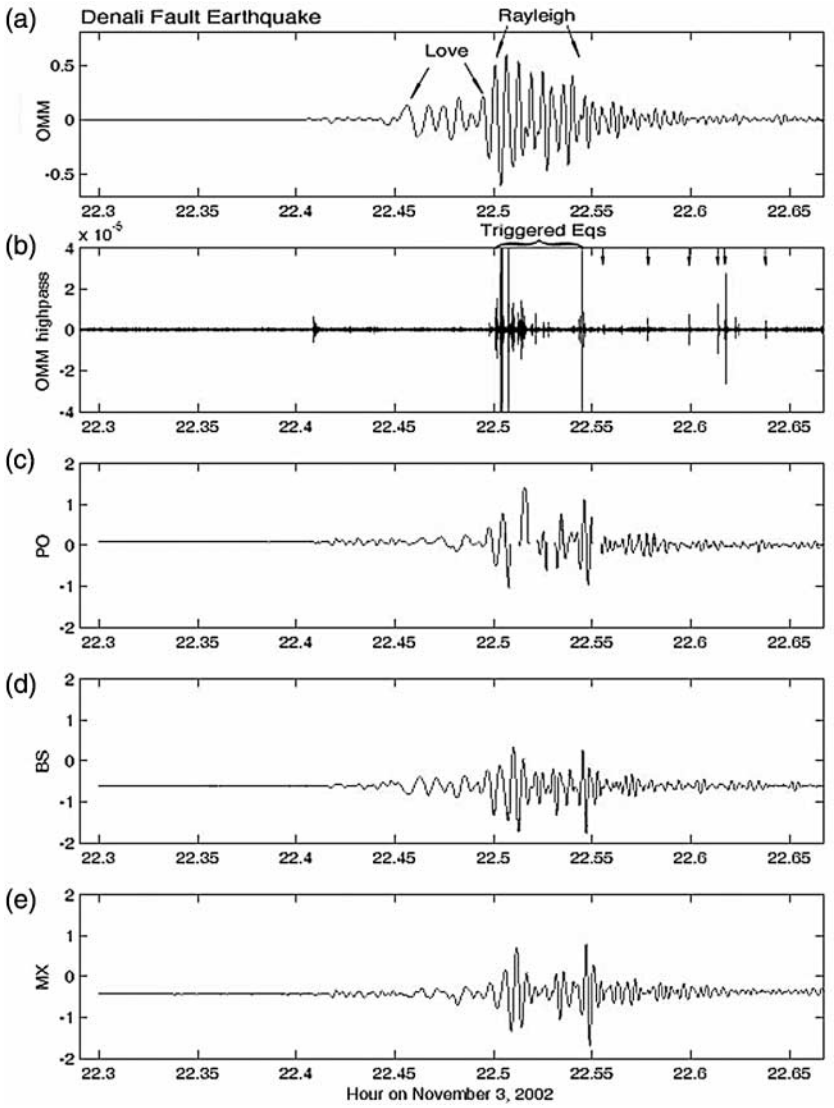

Figure 4. Twenty-two minute time history starting just before the first *P*-wave arrival in Long valley caldera from the 3 November 2002 M_w 7.9 Denali fault earthquake of (a) broadband seismic velocity from OMM, (b) high-pass filtered data from the broadband station OMM east–west component showing the occurrence of local triggered events in relation to the Love and Rayleigh waves, (c) borehole strain from PO, (d) borehole strain from BS, and (e) borehole strain from MX. Strain units are microstrain. Velocity units are cm/sec. Data gaps in the PO record indicate missing data.

While it is clear from these data that Rayleigh-wave amplitude plays a role in the triggering process, amplitude alone appears not to be the sole cause since local earthquakes, such as from the 1986 *M* 6.2 Chalfant and other local earthquakes, produce peak-to-peak dynamic strains comparable to those from the Denali fault earthquake without any apparent triggering effects. The frequency content of seismograms from local earthquakes is, of course, much higher than that from teleseismic events. Thus, it is likely that the triggering process is sensitive to frequency content of the teleseismic wave train. Clearly this is not well understood since Gomberg and Davis (1996) propose triggering by high-frequency waves and others (Anderson *et al.*, 1994; Brodsky and Prejean, 2003) propose triggering by low-frequency waves. Because we have broadband strain data recorded on several strainmeters from teleseismic earthquakes with about the same magnitude and distance both during periods when triggering occurred and when it did not, we can make some initial comments regarding frequency dependence of triggering in the Long Valley region.

Figure 5 shows the power spectra plots for the MX straingram for both the M_w 7.9 Denali fault earthquake and the 25 September 2003 *M* 8.3 Hokkaido earthquake. Most of the power contained in both of these spectra occurs between 0.03 and 0.2 Hz (30 sec to about 5 sec) with a peak of about 0.07 Hz (14 sec). The frequency content is similar for both, while the peak power for the larger Hokkaido earthquake, which occurred at more than twice the epicentral distance of the Denali fault earthquake, is slightly lower than that for the Denali fault earthquake. Similar spectral content was also observed in data from other strainmeter sites in California. These sites are in transpressional environments that had no triggered deformation or seismicity for the Denali fault earthquake or any other large teleseismic earthquake. Thus, triggering can occur for large-amplitude surface wave with dominant frequencies of about 0.07 Hz (e.g., 1992 *M* 7.2 Landers [10 microstrain], 1999 *M* 7.1 Hector Mine [3 microstrain], 2002 *M* 7.9 Denali fault [2 microstrain]). It also may not (e.g., 2003 *M* 8.3 Hokkaido, 1992 *M* 7 Petrolia, 1989 *M* 6.9 Loma Prieta, 1994 *M* 6.7 North-

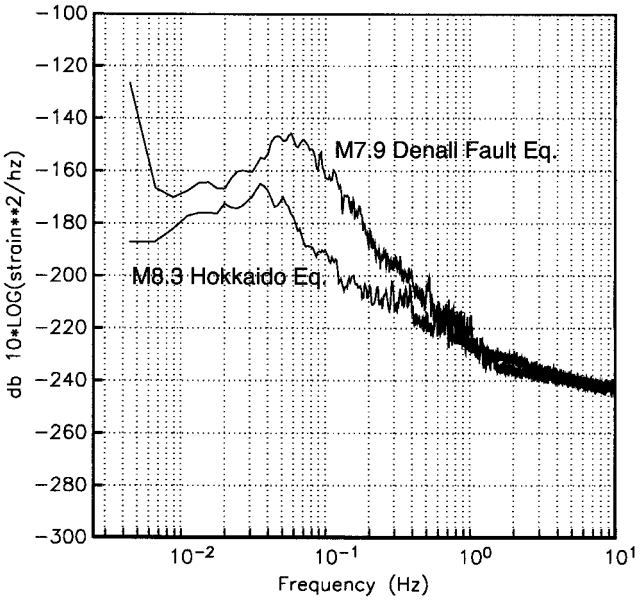

Figure 5. Power spectra of straingrams from the MX strainmeter produced by the 3 November 2002 M_w 7.9 Denali fault earthquake and the 25 September 2003 *M* 8.3 Hokkaido earthquake in the Long Valley caldera. Units are in dB referenced to 1 strain^2/Hz.

ridge) even though peak amplitudes may be larger (10 microstrain for *M* 6.9 Loma Prieta) or slightly smaller (0.3 microstrain for *M* 8.3 Hokkaido) than those for the Denali fault earthquake.

With this observational background, it is important to attempt to isolate which of the various time-dependent physical processes (or combination of processes) is responsible for triggering. These processes include fluid diffusion, rate/state friction, hydrothermal system changes, and bubble growth within magmatic systems (see details in Anderson *et al.*, 1994; Linde *et al.*, 1994; Hill *et al.*, 1995; Johnston *et al.*, 1995, Gomberg and Davis, 1996; Gomberg *et al.*, 1998; Perfettini, 2003).

Deformation Source Model

We have too few strain observations for a unique determination of the source parameters of the triggered strain event. We have tried to determine a plausible source by (1) assuming uniform slip and opening on an equidimensional planar source ($L = W$) centered beneath the triggered seismicity and (2) using the method of Marquardt (1963) for least-squares estimation of the unknown parameters, strike, depth, and opening with Okada's (1985) formulation for the surface deformations due to a dislocation embedded in an elastic half space. We also carried out a forward model search through several thousand parameter choices (strike, dip, slip, and opening) to verify the validity of the solution and to search for alternative solutions. Details of the best solution ($\chi^2 = 35$) obtained are shown in Figure 6. The moment release was 10^{16} N m on a N10°E trending extensional fault dipping 35° to the east and centered at a depth of 8 km with roughly equivalent dip-slip and opening (50 cm and 40 cm respectively). The fault strikes toward the center of MM and is consistent with the occurrence of a triggered small radial dike. While other solutions are certainly possible, this solution is generally compatible with the tectonics of the region (Bailey *et al.*, 1976). Approximate north–south extensional/normal faulting is common throughout the western part of the caldera although the tectonics on the south side of active MM is probably complex. The moment release is equivalent to a *M* 4.3 earthquake and is more than three orders of magnitude larger than the cumulative seismic moment for the triggered seismicity (5×10^{19} N m).

Also show in Figure 6 is a contour plot of best-fitting dilational strain field for this solution. Note that in this figure, extension is positive. The very small positive signal at BS constrains the strike of the source, while the N5°E dip is required to fit the asymmetry of the observations (130 nanostrain at PO and −51 nanostrain at MX) at approximately equal distances from the source. The source depths of the triggered seismicity are constrained by the *S-P* times to be between 1 km of 4 km and therefore appear to be at a shallower depth than the deformational event. It is not clear how the shallower seismicity was triggered by the deformation since we do not know the focal mechanism of the events and cannot say how the change in stress due to the silent slip event caused failure.

Discussion

Stress cycling during the arrival of the Rayleigh waves from the M_w 7.9 Denali fault earthquake triggered deformation and microseismicity beneath MM on the rim of Long Valley caldera. The onset of deformation, as recorded on three borehole dilational strainmeters located on the north, south, and west side of the caldera, began during the first Rayleigh wave-arrivals for which the peak-to-peak strains were about 2 microstrain (corresponding to peak stresses of about 0.06 N m). The deformation evolved in the next 10–15 min during the passage of the Rayleigh wave train. At the end of this time, permanent strain offsets were recorded on all instruments. Some 60 microearthquakes occurred over a 15-min time interval starting at the same time as the strain event in a tight cluster beneath the southern side of MM, a young volcano on the southwestern rim of Long Valley caldera. The triggered microseismicity appears to be related to the deformational event (slow or silent earthquake) and rapidly decays away with time after the deformation is complete.

Remotely triggered deformation and seismicity has occurred before in the Long Valley region, and triggered seismicity has occurred in other volcanic, geothermal and extensional regions (Hill *et al.*, 1993; Gomberg and Davis, 1996; Moran *et al.*, 2003; Prejean *et al.*, 2004). The Long

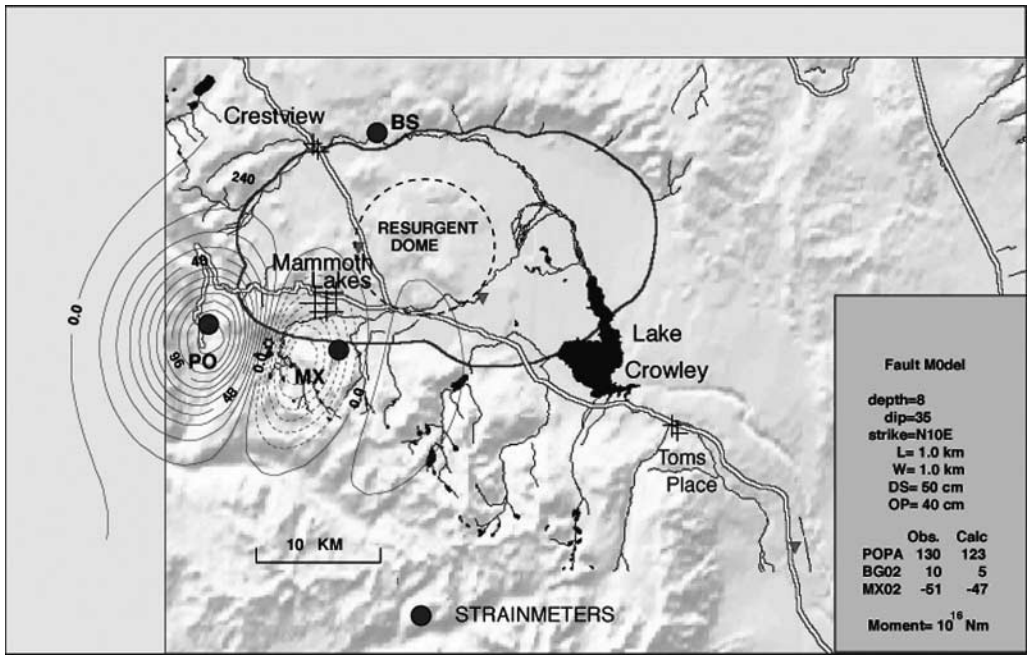

Figure 6. Contour plot of dilational strain due to best-fitting model (see text) of triggered slip in Long Valley caldera generated by the 3 November 2002 M_w 7.9 Denali fault earthquake. The model details and agreement between the observed and calculated strains are included in the table. Contour intervals are 16 nanostrain. Solid and dashed lines represent extensional and compressional dilatations, respectively.

Valley region, however, is the only place with both high-resolution strain and seismic instrumentation that can provide a more complete data related to the physics of triggering. For other sites in California with similar instrumentation, primarily in transpressional stress regimes along the San Andreas fault (Fig. 1), no remotely triggered deformation or seismicity has been observed, although slow earthquakes have been observed at several locations (Johnston *et al.*, 1987a, 1987b; Linde *et al.*, 1996; Johnston and Linde, 2002). Major earthquakes that produced triggered deformation and seismicity in the Long Valley region include the 1992 *M* 7.4 Landers earthquake and the 1999 *M* 7.2 Hector Mine earthquake. It is important to note, however, that other similar magnitude earthquakes such as the 1989 *M* 6.9 Loma Prieta earthquake, the 1992 *M* 7 Petrolia earthquake, and the 1994 *M* 6.7 Northridge earthquake did not produce a triggered response in Long Valley caldera even though the peak-to-peak strain amplitudes were similar to those from Hector Mine and Denali fault earthquakes.

What conditions favor remote triggering? Because geothermal, volcanic, and regions of extensional tectonics appear to be particularly susceptible to remote triggering, suggested processes have included triggered outgassing of magmas or hydrothermal fluids (Linde *et al.*, 1994; Brodsky *et al.*, 1998), changes in rate and state dependent friction (Gomberg and Davis, 1996; Gomberg *et al.*, 1998; Voisin, 2002; Perfettini *et al.*, 2003), failure and diffusion from overpressured hydrothermal reservoirs (Johnston *et al.*, 1995). Each of these processes may be sensitive to enhanced dynamic stress amplitudes associated with rupture directivity (Hill *et al.*, 1993; Gomberg *et al.*, 2004) and frequency dependence of the process (Gomberg and Davis., 1996; Brodsky and Prejean, 2003).

The data presented here suggest that, for this example of remote triggering, surface-wave amplitude is an important factor in the triggering process. The strain process began with the largest wave amplitude and it stopped after about 10 min when the Rayleigh-wave amplitude dropped below about 0.5 microstrain at the end of the Rayleigh wave train. This threshold level is just below the peak-to-peak dynamic strain from the 2003 Hokkaido earthquake for which no triggering occurred.

The rapidity of the triggering process is an important parameter. When deformation triggering from the Denali fault earthquake occurs, it began quickly and ended just as quickly. This would argue against substantial fluid flow on scales of kilometers associated directly with the process (Brodsky and Prejean, 2003). We note that the Denali triggering episode is distinctly different from that observed associated with the 1992 Landers earthquake (Linde *et al.*, 1994; Hill *et al.*, 1995; Johnston *et al.*, 1995) where exponential transient responses with a similar two-day time decay were observed in each of the strain, tilt, and cumulative seismicity records spanning several tens of kilometers of Long

Valley caldera. The response for the 1999 Hector Mine earthquake was similar to the Denali fault earthquake response except that the triggered deformation occurred under the north flank of MM and the triggered seismicity did not start until 20 min after the strain offsets occurred with the Rayleigh-wave arrivals. Swarm activity associated with dike intrusion occurred under both the north and south flanks of MM during the 1989 intrusive activity (Hill *et al.*, 1990), and this may have primed the region for future triggering episodes. Thus it would appear that different triggered responses occur in different places in Long Valley caldera and that physical processes may vary from one triggering episode to the next. The primary requirement seems to be that some low-frequency threshold strain amplitude is exceeded in a region at the point of failure.

There is not a clear correspondence between individual peaks (troughs) in the teleseismically generated dilational strain waveforms (Fig. 4) and microearthquake occurrence, although the initial earthquakes do appear to occur during an extensional phase of the Rayleigh wave. Instead, the earthquakes appear to be related to the local triggered deformational event. Thus, interaction between the Rayleigh wave stress/strain tensor and the stress state in Long Valley caldera appears not to be a direct factor in triggering microearthquakes.

Does frequency sensitivity play a part in the triggering process? The fact that triggering occurs during the surface wave train for teleseismic earthquakes but not for local earthquakes with the same peak-to-peak strain amplitudes but much higher frequency content suggests this is the case, as argued by Brodsky and Prejean (2003) and Prejean *et al.* (2004). The dominant frequencies associated with the teleseismic wave arrivals range from 0.03 to 0.07 Hz whereas those for local earthquakes are much higher. At these periods (15–30 sec), the teleseismic wavelengths are about 30–60 km. This may be important since this is comparable to the dimension of the caldera and may result in a caldera resonance response that, in turn, could result in deformation and microseismic triggering effects. However, if resonance does occur it is small since the amplitudes of Rayleigh waves at other sites in California are similar to those observed in Long Valley. Furthermore, similar frequencies are observed for other earthquakes that did not cause triggering. More subtle effects such as fluid flow with a diffusion time constant comparable to teleseismic wave periods (Brodsky and Prejean, 2003) may play a role but require fracture permeabilities to be 10^{-12} m^2 for length scales of less than a few hundred meters and viscosities of 10^{-4} Pa sec (water) for the diffusion time constants to be short enough (sec).

The strain offset data can be modeled with a simple fault model that is reasonably consistent with the tectonics of the region. While other models may be fit to these data, what is clear is that, whatever model is used, the triggered aseismic moment release is far larger than the triggered seismic moment release. This has been true for all three episodes of triggering in the Long Valley caldera region. Thus triggered microseismicity may result from the deformation events. Detection of further remotely triggered deformation and microseismicity activity for which we have both high-resolution strain and broadband seismic detection capability is clearly needed to further clarify some of these issues.

Conclusions

1. Triggered microseismicity and coseismic strain changes were recorded on seismometers and strainmeters in Long Valley caldera during teleseismic surface-wave arrivals from the 3 November 2002 M_w 7.9 Denali fault earthquake. The strain offsets far exceed expectations from models of static stress change from the Denali fault earthquake source at this epicentral distance (3460 km). Rather, both the deformation and microseismicity appear to result from activity triggered beneath MM by the Denali fault earthquake surface waves.

2. The deformation event was triggered at 22:30 UTC during the first Rayleigh wave arrivals. These were recorded with peak-to-peak amplitudes of about 2 microstrain and periods of about 15 sec on the three borehole dilatometers. The Rayleigh waves are the most dominant phase in the surface wave train. Following onset, the deformation event continued for the next 10 min. The microseismicity triggered under MM started approximately with the deformation and continued on for 5 min after the deformation was complete. Comparable teleseismic amplitudes produced deformation and microseismic triggering during the 1992 Landers and the 1999 Hector Mine earthquakes. However, other teleseismic earthquakes with similar Rayleigh-wave amplitudes (such as the 1989 Loma Prieta, the 1992 Petrolia, and the 1994 Northridge earthquakes) and other large local earthquakes (such as the 1986 *M* 6.2 Chalfant earthquake) did not produce triggering. Wave amplitudes alone are apparently not enough to produce triggering and interaction between these waves and the state of stress and failure of faults and fluid-filled chambers in the caldera is poorly understood.

3. Sensitivity to low-frequency teleseismic surface waves does seem to be a necessary but not sufficient requirement for triggering. While the dimensions of the caldera are such that the dominant frequencies (0.03–0.07 Hz) might cause a resonant response, this is not evident in the comparative strain observations inside and outside the caldera. The rapid onset and cessation of the triggered deformation from the Denali fault teleseismic waves argues against a significant role for fluids flow on scales of kilometers in the physical process for this earthquake (Brodsky and Prejean, 2003). More subtle frequency dependence of friction coefficients of faults (Gomberg and Davis, 1996; Voisin, 2002) triggered when loading amplitude exceeds 0.04 MPa could be the most likely physical process responsible for the Denali fault earthquake triggering episode.

4. Static strain offsets produced by the deformational event recorded on just three strainmeters are insufficient to allow a unique independent determination of the local deformational source mechanism. However, by assuming simple geometry and restricting the location to the microseismic epicenters, we are able to invert for plausible source parameters consistent with the available deformation data and to search through various model parameters in a forward modeling sense for other possible models. The best fit to the data results from a model in which triggered slip and intrusive opening on a N10°E striking normal fault centered at a depth of 8 km beneath the triggered microseismicity with a moment of 10^{16} N m, or the equivalent of a M 4.3 earthquake. As with previous triggering episodes in Long Valley, this moment release far exceeds that released by the triggered microseismicity.

Acknowledgments

We thank Paul Bodin, John Langbein, Emily Brodsky, and an anonymous reviewer for useful comments. The dilatometers were installed with help from Bob Mueller, Doug Myren, and others who participated in the installation and provided technical support. Tom Burdette, Dave Croker, and Dave Reneau installed the 24-bit telemetry system that allowed observation of high-frequency recordings of strain and seismic velocity data. We are indebted the University of Nevada for the data from OMM and to Ken Smith for discussions about possible resonance effects.

References

Anderson, J. G., J. N. Brune, J. N. Louie, Z. Yueua, M. Savage, G. Yu, Q. Chen, and D. dePolo (1994). Seismicity in the western Great Basin apparently triggered by the Denali, California, earthquake, 28 June 1992, *Bull. Seism. Soc. Am.* **84,** 863–891.

Bailey, R. A., G. B. Dalrymple, and M. A. Lanpere (1976). Volcanism, structure and geochronology of Long Valley caldera, Mono County, California (1976), *J. Geophys. Res.* **81,** 725–744.

Brodsky, E. E., and S. G. Prejean (2003). Frequency dependent dynamic triggering, *Trans. Am. Geophys. Union* **84** (fall meeting suppl.). Abstract S31G-05.

Brodsky, E. E., B. Sturtevant, and H. Kanamori (1998). Volcanoes, earthquakes and rectified diffusion, *J. Geophys. Res.* **103,** 23,827–23,838.

Eberhart-Phillips, D., P. J. Haeussler, J. T. Freymueller, A. D. Frankel, C. M. Rubin, P. Craw, N. A. Ratchkovski, G. Anderson, A. J. Crone, T. E. Dawson, H. Fletcher, R. Hansen, E. L. Harp, R. A. Harris, D. P. Hill, S. Hreinsdóttir, R. A. Jibson, L. M. Jones, R. Kayen, D. K. Keefer, C. F. Larsen, S. C. Moran, S. F. Personius, G. Plafker, B. Sherrod, K. Sieh, N. Sitar, and W. K. Wallace (2003). The 2002 Denali fault earthquake, Alaska: a large magnitude, slip-partitioned event, *Science* **300,** 1113–1118.

Gomberg, J., and S. Davis (1996). Stress/strain changes and triggered seismicity at the Geysers, California, *J. Geophys. Res.* **101,** 733–749.

Gomberg, J., N. M. Beeler, M. L. Blanpied, and P. Bodin (1998). Earthquake triggering by transient and static deformation, *J. Geophys. Res.* **103,** 24,411–24,426.

Gomberg, J., P. A. Reasenberg, P. Bodin, and R. A. Harris (2001). Earthquake triggering by seismic waves following the Landers and Hector Mine earthquakes, *Nature* **411,** 462–465.

Gomberg, J., P. Bodin, K. Larson, and H. Dragert (2004). The fundamental process of earthquake nucleation by transient deformations revealed by the M 7.9 Denali, Alaska earthquake, *Nature* **427,** 621–624.

Haeussler, P. J. (2003). Surface rupture and revised slip distribution on the Denali and Totschunda faults from the M 7.9 Denali fault earthquake, *Trans. Am. Geophys. Union* **84** (fall meeting suppl.). Abstract S11B-02.

Hill, D. P., W. L. Ellsworth, M. J. S. Johnston, J. O. Langbein, D. H. Oppenheimer , A. M. Pitt, P. A. Reasenberg, M. L. Sorey, and S. R. McNutt (1990). The 1989 earthquake swarm beneath Mammoth Mountain, California: an initial look at the 4 May through 30 September activity, *Bull. Seism. Soc. Am.* **80,** 325–339.

Hill, D. P., P. A. Reasenberg, A. Michael, W. J. Arabaz, G. Beroza, D. Brumbaugh, J. N. Brune, R. Castro, S. Davis, D. dePolo, W. L. Ellsworth, J. Gomberg, S. Harmsen, L. House, S. M. Jackson, M. J. Johnston, L. Jones, R. Keller, S. Malone, L. Munguia, S. Nava, J. C. Pechmann, A. Sanford, R. W. Simpson, R. B. Smith, M. Stark, M. Stickney, A. Vidal, S. Walter, V. Wong, and J. Zollweg (1993). Seismicity remotely triggered by the magnitude 7.3 Landers California earthquake, *Science* **260,** 1617–1623.

Hill, D. P., M. J. S. Johnston, and J. O. Langbein (1995). Response of Long Valley caldera to the $M_w = 7.3$ Landers, California, earthquake, *J. Geophys. Res.* **100,** 12,985–13,005.

Husker, A. L., and E. E. Brodsky (2004). Triggered seismicity in Idaho and Montana: a window into the geologic context for seismic triggering, *Bull. Seism. Soc. Am.* **94,** no. 6B, S310–S316.

Johnston, M. J. S., R. D. Borcherdt, M. T. Gladwin, G. Glassmoyer, and A. T. Linde (1987a). Fault failure with moderate earthquakes, *Tectonophysics* **144,** 189–206.

Johnston, M. J. S., R. D. Borcherdt, M. T. Gladwin, G. Glassmoyer, and A. T. Linde (1987b). Static and dynamic strain during the M_L 5.9 Banning, California, earthquake on July 8, 1986, *Trans. Am. Geophys. Union* **68,** 1244.

Johnston, M. J. S., D. P. Hill, A. T. Linde, J. Langbein, and R. Bilham (1995). Transient deformation during triggered seismicity from the June 28, 1992, $M_w = 7.3$ Landers earthquake at Long Valley volcanic caldera, California, *Bull. Seism. Soc. Am.* **85,** 787–795.

Johnston, M. J. S., D. P. Hill, and A. M. Pitt (2000). Strain transient recorded in the Long Valley caldera during triggered seismicity from the October 16, 1999, M 7.1 Hector Mine, California, earthquake, *Trans. Am. Geophys. Union* **81,** WP1384.

Johnston, M. J. S., and A. T. Linde (2002). Implications of crustal strain during conventional, slow and silent earthquakes, in *International Handbook of Earthquake and Engineering Seismology*, Vol. 81A, Academic Press, New York, 589–605.

Linde, A. T., M. T. Gladwin, M. J. S. Johnston, R. L. Gwyther, and R. Bilham (1996). A slow earthquake near San Juan Bautista, California, in December, 1992, *Nature* **383,** 65–68.

Linde, A. T., I. S. Sacks, M. J. S. Johnston, D. P. Hill, and R. G. Bilham (1994). Increasing pressure from rising bubbles as a mechanism for remotely triggered seismicity, *Nature* **371,** 408–410.

Moran, S. C., D. R. Zimbelman, and S. D. Malone (2003). A model for the magmatic-hydrothermal system at Mount Rainier, Washington, from seismic and geochemical observations, *Bull. Seism. Soc. Am.* **61,** 425–436.

Marquardt, D. W. (1963). An algorithm for least-squares estimation of nonlinear parameters, *J. Soc. Ind. Appl. Math.* **11,** 431–441.

Okada, Y. (1985). Surface deformation due to shear and tensile faults in a half-space, *Bull. Seism. Soc. Am.* **75,** 1135–1154.

Okada, Y. (1992). Internal deformation due to shear and tensile faults in a half-space, *Bull. Seism. Soc. Am.* **82,** 1018–1040.

Pankow, K. L., W. J. Abarasz, J. C. Pechmann, and S. J. Nava (2004). Triggered seismicity in Utah from the 3 November 2002, Denali fault earthquake, *Bull. Seism. Soc. Am.* **94,** no. 6B, S332–S347.

Perfettini, H. J., H. J. Schmittbuhl, and A. Cochard (2003). Shear and normal load perturbations on a two-dimensional continuous fault: dynamic triggering, *J. Geophys. Res.* **108,** doi 10.1029/2002JB001969.

Prejean, S., D. P. Hill, S. Hough, M. Johnston, S. Malone, D. Oppenheimer, M. Pitt, and K. Richards-Dinger (2004). Remotely triggered seismic-

ity on the United States west coast following the M_w 7.9 Denali fault earthquake, *Bull. Seism. Soc. Am.* **94,** no. 6B, S348–S359.

Sacks, I. S., S. Suyehiro, D. W. Evertson, and Y. Yamagishi (1971). Sacks-Evertson strainmeter, its installation in Japan and some preliminary results concerning strain steps, *Papers Meteorol. Geophys.* **22,** 195–207.

Silverman, S., C. Mortensen, and M. J. S. Johnston (1989). A satellite based digital data system for low-frequency geophysical data, *Bull. Seism. Soc. Am.* **79,** 189–198.

Tamura, Y., T. Sato, M. Ooe, and M. Ishiguro (1991). A procedure for tidal analysis with a Bayesian information criterion, *Geophys. J. Int.* **104,** 507–516.

Voisin, C. (2002). Dynamic triggering of earthquakes: the nonlinear slip-dependent friction case, *J. Geophys. Res.* **107,** doi 10.1029/2001 JB001121.

U.S. Geological Survey
345 Middlefield Road, MS977
Menlo Park, California 94025

Manuscript received 7 January 2004.